中国科学院紫金山天文台 博士后流动站
博士后出站研究报告

活动星系中的热气体反馈

张水乃
合作导师：纪丽 研究员

2014 年 12 月 26 日

Purple Mountain Observatory, Chinese Academy of Sciences

Post-doctoral station, Research Report

Hot Gas Feedback in Energetic Galaxies

Shui-Nai Zhang
Co-Surpervisor: Dr. Li Ji

December 26, 2014

引言

在宇宙演化过程中，星系的变动往往伴随着剧烈的高能现象，例如进入活动星系核(AGN)或者星暴阶段，又如星系绕转乃至并合。X射线及紫外波段的观测打开了这扇窗口，因为高能现象通常会产生大量的热气体（$10^5 - 10^8$ K）从而在高能波段可见。从中心亚pc尺度量级的外流，到几kpc量级的星系风，甚至几十kpc量级的星系周边热气体环绕带，这些弥散在四处的热气体为我们带来了对星系演化的全新认识。

以眼所见，我们尝试去理解这些热气体的起源机制以及对周围环境的交互作用。光谱学研究表明这些热气体可能处于截然不同的物理状态，从而揭示出星系中各异的物理过程。然而，不同过程所展示的区别，即使在光谱中，往往也仅有很细微的区别。很多时候并不能在CCD的X射线光谱中得到展现，但所幸高分辨率光谱已经足够揭示某些细微之处。通过比较金属元素众多原子跃迁产生辐射的强弱，恰巧这些跃迁多数在高能波段，即可推测热气体的物理和化学性质。若加上更高速度分辨率的UV光谱，更可以了解其动力学乃至几何形态。

只是，了解不同物理过程应有的光谱辐射特征，才是一把钥匙，通过比较观测而发现细微的不自恰之处，从而甄别热气体的起源机制等。这些年，或实验或理论计算的原子数据被逐步的收集比较，变成适合用于天文的格式。而不同的物理机制模型，也变得完善，配合新的原子数据库，能生成可与高分辨率观测 直接比较的光谱。

在博后期间，基于科学驱动，协助合作者开发和更新两种软件，并将其首次运用到河外星系的辐射机制研究中，得到全新的结果。一个是对星系风的原型，星暴星系M82的电离外流的研究；一个是对Seyfert I型星系Mrk290的核区电离外流的研究。

软件之一是电荷交换(CX)的辐射光谱生成软件。我们的研究需求促使合作者开发出多次CX的模式，现已作为模型的基本模式。这也是我们首次将CX光谱模型应用到河外星系中去。在星暴星系的观测到的软X射线辐射中，CX被认为会在冷热气体的交界处产生显著的贡献。了解CX在其中的贡献，才可以无误的测量热气体的热力学和化学性质，以及对冷热气体的相互作用提供诊断。使用这最新的CX模型加上充满空间的单温等离子体热谱模型，我们分析了M82的XMM-Newton/RGS光谱。模型精确的拟合了观测光谱，对单根辐射线的流量误差基本在25%以内。CX过程不仅极大的增强了类氦离子的禁线辐射，对类氢离子Lyα跃迁的流量贡献 也很大，比如对C VI、O VIII和N VII辐射的贡献都超过一半。在RGS的6-30Å的波段，CX的辐射贡献足占了四分之一。我们推断CX过程中在冷热气体交界面处离子的碰撞率为$3.2 \times 10^{51}\,\mathrm{s}^{-1}$，或者有效碰撞截面为$2 \times 10^{45}\,\mathrm{cm}^2/v_{500}$，其中$v_{500}$是以$500\,\mathrm{km\ s}^{-1}$为单位的两相气体之间的相对速度。这个面积，比双锥结构的星系热

气体外流的几何截面要大上一个量级， 表明了两相气体之间的充分混合，自然的与外流的质量加载过程关联起来。 通过考虑CX过程之后，热气体的最佳拟合温度为0.6 keV， 而金属丰度与太阳值相差不大，其中O和Fe似乎被尘埃大量消耗。 我们也进一步展示，同样的CX加热等离子体的模型也能很好的描述外流的Cap区域的 EPIC-pn光谱。

软件之二是升级到可在X射线至光学波段使用的XSTAR。 我们模拟了Mrk290的HST/COS的整个光谱，从而分析外流的内禀紫外吸收。 内禀吸收的光致电离模型，加上AGN的宽窄线区的辐射模型以及本地高速云和星际介质 的吸收模型，可以准确的拟合光谱； 这些模型都由XSTAR生成。 这也是首次物理的拟合整条COS光谱。 一共有三个内禀吸收体被证认出来。 其中两个是通过N V和C IV双线发现，它们在光谱中有66 km s^{-1}的分隔； 而第三个是通过Lyα的额外吸收发现的。 这三个吸收体与我们之前从X射线波段的Chandra观测发现的中低电离程度的温吸收体在各个方面包括外流速度、电离程度和柱密度都非常类似， 使人想起吸收气体在两个波段一一对应的关系。 于是两个波段的信息可以被综合起来限制紫外波段三个温吸收体的性质。 较小的湍动速度($v_{turb} \lesssim 100$ km s^{-1})支持我们从X射线研究得出的结论， 即吸收体起源于尘埃环内层的热蒸发。 考虑三个温吸收体的覆盖因子为$\sim$65%，我们发现吸收体的长度和厚度大体相当， 暗示着其几何形态更像是云团状的而非扁平层流状气体。 另外我们还发现，在宽线区中当云团非常接近黑洞时，覆盖率会增高。

而使用新的XSTAR的意义，不仅联合了两个波段， 还使得不同时段的观测信息可以被综合起来。 加上Mrk290的FUSE观测，发现对其吸收体的观测横跨从2000到2009的十年。 我们证明其中三个重要的吸收体在这十年始终存在，于是实现了对简单纯粹的温吸收体的 最长时间的监测。 同时，我们发现在这10年，Mrk290近在2003-2004年有一次大的光度增强。 这也为我们研究AGN活动对外流气体的影响提供了宝贵资料。

结合合作者正在开发的非平衡态碰撞电离光谱生成软件与光致电离光谱生成软件XSTAR， 我们也正在探索非平衡态光致电离情形，并将其运用到AGN星系NGC4151中去。 这个AGN在之前的某个时间段可能有超Eddington的吸积，其光度甚至照亮了整个窄线区。 我们可以通过分析窄线区的X射线光谱来推断AGN暴发时的状况等等。

最后是研究环绕M31的弥散气体。 这些暗弱的弧状气体是首次被观测到，是本星系群中星系作用留下的遗迹。 我们将通过研究这些气体在紫外波段的吸收线来研究其物理化学和动力学性质。

以上即为博后期间完成和正在进行的工作。

Abstract

During evolution of the universe, transitions of galaxies usually accompany severe energetic phenomenons, such as the stages of active galactic nuclei (AGN) or star burst, and the stages when the galaxy pair is rotating with each other or even begins to merge. Observations in the X-ray and UV bands opened this window, because an enormous amount of hot gas ($10^5 - 10^8$ K) are produced in the transitions and thus become visible in these bands. From the sub-pc scale outflows in the center of galaxies, several kpc scale galactic wind, to several ten kpc scale hot gas belt around galaxies, the diffuse hot gas bring us completely new knowledges about the evolution of galaxies.

Based on things we see, we try to understand the origin of the hot gas, its mechanism, and its interplay with the environments. The spectral research suggests distinctive physical states of the hot gas, revealing various processes in the galaxies. However, the differences of these various precesses, even in spectra, could be very tiny. Most time they can not be revealed in CCD X-ray spectra, but may show some clues in high resolution spectroscopic studies. Comparing the intensities of huge atomic transitions of metal elements, most of which happens at high energy band, we can speculate the physical and chemical properties of the hot gas. Plus the ultraviolet (UV) spectra with higher velocity resolution, the dynamics and even the geometries can be derived.

To understand remarkable spectral features of multiple physical processes, is the key. We compare observations and check for any small particular issues that is in disagreement, to distinguish different origins of the hot gas. These years, atomic data from either laboratory or theoretical studies are collected, compared, chosen, and finally formatted to the form that is suitable for astronomy. Many models for different physical mechanisms are nicely improved, together with the new atomic database, producing synthetic spectra that can be compared directly with observed high resolution spectra.

During the period of postdoc, driven by scientific motivation, I cooperates with my coauthors to develop and update different codes, and used two of them for the first time in the radiation research of ex-galaxies, achieving some new results. One is in the study of the ionized outflow of starburst galaxy M82 which is the prototype of galactic scale superwind; another is for the study of the nucleus ionized outflow of a Seyfert I galaxy, Mrk 290.

One code is used to produce spectra of charge exchange (CX) process. Our research required a new multiple CX mode, which is now the standard mode of this code. This is also the first time we apply this CX spectra inside the situation of ex-galaxies. In the observed soft X-ray emission of starburst galaxy M82, CX contributes significantly

at the interaction surfaces of the hot and cold gas. Understanding the contribution of CX, we can reasonably measure the thermal and chemical properties of the hot gas, and supply the diagnostics for the interaction of hot and cold gas. We analyze the XMM-Newton/RGS spectrum of M82, using a newly developed CX model, combined with a single-temperature optically-thin thermal plasma, characterizing the volume-filling hot gas, as well as a power law, accounting for point-like source-dominated continuum. This simple model combination fits the spectrum well to an accuracy of matching individual emission features typically within 25%. The CX process is largely responsible for not only the strongly enhanced forbidden lines of the Kα triplets of various He-like ions, but also good fractions of the Lyα transitions of C VI ($\sim$ 87%), O VIII and N VII ($\gtrsim$50%) as well. About a quarter of the X-ray flux in the RGS band 6-30 Å originates in the CX. We infer an effective ion flux of 3.2×10^{51} s^{-1} undergoing CX at hot and cool gas interfaces. Assuming a relative speed of 500 km s^{-1}, we may further estimate the total effective area of the interface area as 15.8×10^{44} cm^2, or about 16 times larger than the cross section of the global biconic outflow of the hot gas from the galaxy. This interface area increase characterizes the turbulent mixing between the two gas phases, indicative of a substantial mass-loading of the hot gas. With the CX contribution accounted for, the best-fitting temperature of the hot gas is 0.6 keV, while its metal abundances are approximately solar, which may again result primarily from the mass-loading. We further show that the same CX/thermal plasma model also gives an excellent description of the EPIC-pn spectrum of the outflow 'cap', projected at 11.6 kpc away from the galactic disk of M82.

The second code is the upgraded XSTAR which is capable to cover from the X-ray band to the optical band with requited resolution. We present a new method to model a HST/COS spectrum, aimed to analyze intrinsic UV absorption from the outflow of Mrk 290, a Seyfert I galaxy. We use newly updated XSTAR to generate photoionization models for the intrinsic absorption from the AGN outflow, the line emission from the AGN broad and narrow line regions, and the local absorption from high velocity clouds and Galactic interstellar medium. The combination of these physical models accurately fit the COS spectrum. Three intrinsic absorbers outflowing with velocities $\sim$500 km s^{-1} are identified, two of which are found directly from two velocity components of the N V and C IV doublets, while the third is required by the extra absorption in the Lyα. Their outflow velocities, ionization states and column densities are consistent with the lowest and moderately ionization warm absorbers (WAs) in the X-ray domain found by Chandra observations, suggesting an one-to-one correspondence between the absorbing gas in the UV and X-ray bands. The small turbulent velocities of the WAs ($v_{\rm turb} \lesssim 100$ km s^{-1}) support our previous argument from the X-ray study that the absorbers originate from the inner side of the torus due to thermal evaporation. Given the covering fractions of $\sim$65% for the three WAs, we deduce that the lengths and the thicknesses of the WAs are

comparable, which indicates that the geometry of WAs are more likely clouds rather than flat and thin layers. In addition, the modeling of the broad line emission suggests a higher covering fraction of clouds when they are very closer to the black hole.

The purpose of using this new XSTAR, is more than combination of the two bands. It combines information from multiple periods. Plus the FUSE observations, we explore the ten-year history of warm absorbers (WAs) in Mrk 290 over the period from 2000 to 2009. One-to-one relation of WAs has been proved between UV and X-ray bands, and part of the absorption over ten years is identified as the same one. The variability of its column density seems to be related to the changes of ionizing luminosity that has a peak between 2003 and 2004. The result gives us precious material for studying the impact of AGN outflows.

The linkup of the new non-equilibrium collisional ionization spectral code developed by my coauthors and the new photoionization spectral code XSTAR, produces the non-equilibrium photoionization spectra. We are exploring the astronomical situations for it, and use it to study an AGN, NGC 4151. This AGN may be at super Eddington accretion state some time ago, the luminosity of which illuminated the whole narrow line region (NLR). By analysis of the X-ray spectrum of the NLR we can infer what happened when the AGN exploded.

And finally, it is the belt-like diffuse gas around M31 that is observed very recently. This gas is believed to be the relic of the rotations and interactions of galaxies in the local group. We are studying the UV absorption lines to reveal its physical and dynamical properties.

The above is what I did and what I'm doing now.

目 录

引言 i

Abstract i

第 一 章 简介 1
§ 1.1 星暴星系中的超级风 1
§ 1.2 AGN中的温吸收外流气体 3

第 二 章 电离气体与模型 7
§ 2.1 电荷交换光谱软件ACX 7
§ 2.2 ACX的诊断分析 8
2.2.1 辐射效率 8
2.2.2 独特的双峰结构 9
§ 2.3 光致电离模型XSTAR 11

第 三 章 星暴星系M82超级风之CX辐射 13
§ 3.1 XMM-Newton数据处理 13
§ 3.2 光谱拟合 14
3.2.1 RGS发射线轮廓模拟 14
§ 3.3 结果 16
§ 3.4 讨论 20
3.4.1 热等离子体的性质 20
3.4.2 冷热气体的交界面 25
3.4.3 Cap区域的独特交界面 26
3.4.4 软X射线与Hα辐射的相关性 27
§ 3.5 结论 28
§ 3.6 Astro-H SXS的光谱模拟 30

第 四 章 活动星系核Mrk 290的双波段温吸收气体 33
§ 4.1 COS数据处理 33
§ 4.2 单个物理组分的光谱分析 34
4.2.1 银河系本地吸收 35
4.2.2 Mrk290的辐射 37
4.2.3 电离外流的吸收 39

§ 4.3 光谱拟合和结果 41
4.3.1 AGN辐射与本地吸收 42
4.3.2 电离外流吸收 44
§ 4.4 讨论 48
4.4.1 温吸收体在双波段的一一对应关系 48
4.4.2 电离外流的几何形态 48
§ 4.5 结论 49
§ 4.6 FUSE数据处理及X射线观测 50
§ 4.7 十年的光度变化 50
§ 4.8 重新拟合XMM-Newton光谱的温吸收 51
§ 4.9 FUSE波段的温吸收 51

第 五 章 后续工作 **57**
§ 5.1 环绕M31的弥散气体 57
§ 5.2 爆发后的AGN遗迹 58

参考文献 **61**

基金与文章 **67**

致谢 **68**

第一章　简介

§1.1　星暴星系中的超级风

Galaxy-scale outflows (sometimes called superwinds) driven by supernovae (SNe) are ubiquitous in starburst galaxies (e.g., Heckman et al. 1990; Heckman 2005). Such outflows represent a primary mechanism of stellar feedback, which injects energetic and chemically enriched materials into the circumgalactic medium or even the intergalactic medium (Veilleux et al. 2005). The outflows consist of multiple phases, including X-ray-emitting thermal plasma (e.g., Bregman et al. 1995; Griffiths et al. 2000), warm ionized gas (Shopbell & Bland-Hawthorn 1998), neutral atomic/molecular gas, and dust (Lehnert et al. 1999; Taylor et al. 2001), as shown in M82---the target galaxy of the present study.

As a prototype starburst-driven outflow, M82 has received some of the most extensive studies of individual galaxies. The salient parameters of the galaxy are listed in Table 1.1. The outflow from the nuclear region of the galaxy extends at least 3 kpc away on both sides from the galactic disk along its minor axis. It is widely assumed that the outflow is driven by volume-filling hot plasma, and cold and warm gases are entrained within the flow (e.g., Chevalier & Clegg 1985). Little is actually known about the origin of the emission lines and hence about the properties of the hot plasma and its interplay with the cool components. The soft X-ray emission ($\sim$0.5--1 keV), in particular, may arise from either the volume-filling hot outflow (Fabbiano 1988; Bregman et al. 1995) or mostly from the cool--hot gas interface with a very low volume-filling factor (?Strickland et al. 2002). Without separating these very different contributions, one cannot determine the energetics, the thermal and chemical properties of the hot plasma, and hence the potential role of the outflow in regulating the evolution of the galaxy and its environment.

High-resolution X-ray spectroscopy offers an opportunity to greatly advance our understanding of galactic outflows. Here we use the XMM-Newton reflection grating spectrometer (RGS) observations of M82 to demonstrate this potential. Although the X-ray emission from the galaxy is extended, the large wavelength dispersion of the RGS still allows us to detect or resolve key individual X-ray emission lines or complexes, such as Kα triplets of He-line ions, with confusion far less than in an X-ray CCD spectrum (e.g., extracted from XMM-Newton/European Photon Imaging Camera (EPIC) data). Indeed,

Table 1.1. Parameters of M82

Parameter	Value	Ref.[a]
R.A.(J2000.0)	09:55:52.7	1
Decl.(J2000.0)	+69:40:46	1
Distance	3.52 Mpc	2
Scale	1.02 kpc arcmin^{-}1	2
Redshift	0.000677	1
Disk inclination	81.°5	3
Star formation rate	$\sim 5\,M_{\odot}\,\mathrm{yr}^{-1}$	4

[a]References. (1) NASA/ IPAC Extragalactic Database (NED, http://ned.ipac.caltech.edu); (2) Jacobs et al. (2009); (3) Lynds & Sandage (1963); (4) Strickland & Heckman (2009).

existing studies with the RGS data have already demonstrated the diagnostic power of the line spectroscopy. In the analysis of a 50 ks RGS observation of M82, Ranalli et al. (2008) found that the O VIII Lyα line and the O VII Kα triplet cannot be appropriately accounted for even with a multitemperature thermal plasma model, and they argued that the O VII triplet may indicate a significant contribution from charge-exchange (CX; Beiersdorfer et al. 2003). This process occurs when an ion captures an electron from a neutral atom or molecule. The captured electron tends to be in an excited state; the subsequent downward cascades can produce emission lines with relative intensities distinctly different from a collisionally excited plasma (Foster et al. 2012). Liu et al. (2012) quantified the CX contributions by analyzing individual line components of the Kα triplets of helium-like O, Ne, and Mg ions. Because of the electron capture, CX contributes more to the line emission from lower ionization states than in an equilibrium thermal plasma; in the case of multiple CX reactions, the emission appears at increasingly lower ionization states. Therefore, the spectral analysis of the emission arising even partly from the CX could lead to very misleading results on the temperature and chemical properties of the plasma, if only its thermal (collisionally excited) emission is considered. CX may also contribute significantly to the enhanced X-ray emission from the so-called outflow Cap, projected at 11.6 kpc away from the galactic disk of M82 (Lallement 2004). This X-ray enhancement coincides with an Hα-emitting filament (Devine & Bally 1999), which is also seen in ultraviolet emission due to

the reflection by dust (Hoopes et al. 2005). Although the X-ray CCD spectra obtained from Suzaku and XMM-Newton observations are well characterized by two-temperature components of optically thin thermal plasma, it has been suggested that some of the observed emission lines could be due to the CX (Tsuru et al. 2007).

In this paper, we take a step further to model the entire RGS spectrum of M82, accounting for both thermal and CX contributions simultaneously. We assume a volume-filling, single-temperature, optically thin plasma in collisional ionization equilibrium, which is responsible for the thermal emission, and an interface of the plasma with cool gas, where the CX occurs. This simple model is particularly motivated by the development of an integrated CX spectral code (Smith et al. 2012). We check how well the RGS spectrum can be fitted with the model and what constraints can be obtained on the effectiveness of the CX process or the effective interface area, as well as the properties of the thermal plasma. We further apply the model to the analysis of an XMM-Newton/EPIC-pn spectrum of the Cap region to check the consistency of the model and to infer the dynamics of the outflow.

§1.2 AGN中的温吸收外流气体

Ionized outflowing gas from the central engines of Active Galactic Nuclei (AGN) has been studied for thirty years (since Halpern 1984). In about 50% of Seyfert I galaxies, outflowing gas is characterized by blue-shifted absorption lines in the UV band (Crenshaw et al. 1999) and/or the X-ray band (Reynolds 1997; George et al. 1998). The gas has a high covering fraction, a total mass exceeding $\sim 10^3\,\mathrm{M}_\odot$, and is outflowing at a rate of $\gtrsim 0.1\,\mathrm{M}_\odot\,\mathrm{yr}^{-1}$ (Kriss 2004). Theoretically, it may have a significant impact on the evolution of the host galaxy, when its kinetic luminosity reaches 0.5% of the bolometric luminosity of AGN (Hopkins & Elvis 2010). A significant fraction of Seyfert I galaxies can reach this criterion (e.g., $\gtrsim$3 in 10 nearby Seyfert I galaxies, Crenshaw & Kraemer 2012). However, a key question that complicates the determination of kinetic luminosity of outflowing gas is its distance from the black hole (BH), and hence its geometry. In only a few sources are the distance and the geometry well constrained through careful studies in recent years (Steenbrugge et al. 2011).

Ideally, it is possible to probe the geometric and physical properties of photoionized outflowing gas by combining the information from UV and X-ray observations (e.g., Costantini 2010). The X-ray absorbing gas contains a multitude of ions with up to $\sim$100 observable transitions in X-ray spectra (e.g., Kaspi et al. 2002). The ionization states cover a large range and overlap with those of the UV absorbing gas. The gas at very high ionization states can only be detected in X-ray spectra, while UV band spectra have advantages in detecting absorption lines from gas at low ionization states and with low column densities.

However, the observations in the two bands do not merely offer the complementarity of a broader-band view of the ionization structure of the plasma. UV observations have significantly higher spectral resolution and so are able to supply better kinematic information by resolving complicated profiles of absorption lines. Components with different velocities can be fully distinguished, and their turbulent velocities can be estimated. If reliable column densities for several ionic species are obtained simultaneously, elemental abundances can be estimated (e.g., Arav et al. 2007). The geometric and physical properties of the outflowing gas can be inferred from the distributions of ionization state, column density, velocity and abundance. Moreover, relative positions of the absorbing gas to different emitting components are easier to be obtained in the UV band. Any variability in the UV and X-ray bands will also constrain on the locations.

It has been proven difficult to perform joint analyses of UV and X-ray spectra, because it is hard to find an one-to-one relation of absorbers between the two bands. The reason is that the ionization level and kinematics of both the UV absorbers and X-ray warm absorbers (WAs) are sometimes difficult to measure, and there is often only partial overlap in the conditions of the two sets of absorbers (Crenshaw et al. 2003). Using recent high spectral-resolution telescopes and instruments, there have been numerous multi-wavelength UV-X-ray campaigns. These provide much insight into the physical conditions in the absorbing outflows. However, a broad understanding of these outflows has yet to emerge, and the relationship between the X-ray and UV absorbing gas is still not understood in many cases. In most cases, UV absorbing gas is likely associated with the X-ray WAs, but frequently one X-ray WA may correspond to a blend of several UV absorbers (e.g., NGC 3516, Kraemer et al. 2002; NGC 4593, Ebrero et al. 2013; 1H0419-577, Di Gesu et al. 2013; Mrk 279, Scott et al. 2004; Mrk 509, Kriss et al. 2012; MR 2251-178, Reeves et al. 2013). In other cases, the absorbing gas may favor a continuous distribution of ionization states in a smooth flow, instead of discrete components (e.g., NGC 5548, Steenbrugge et al. 2005; NGC 7469, Scott et al. 2005; IRAS, 13349+2438 Lee et al. 2013). In other cases, variability of the absorbers interfere with identification (e.g., NGC 3783, Gabel et al. 2003, a & b; NGC 4051, Collinge et al. 2001). In particular cases, e.g. in NGC 4151, strong emission lines in the X-ray band contaminate the detection of WAs at lower ionization states (Kraemer et al. 2005). In summary, absorbers are complicated in the both bands, and their information is not easy to be combined.

In this work, we focus on a nearby Seyfert I galaxy, Mrk 290, which shows an extremely simple absorption system in the UV band (Kriss 2002). Meanwhile, only three X-ray WAs were detected in its outflow using the Chandra High Energy Transmission Grating Spectrometer (HETGS) in our previous paper (Zhang et al. 2011, hereafter Z11). This is therefore a relatively clean case with advantages for the illustration of joint analysis. Mrk 290 fortunately has simultaneous observations with Chandra and FUSE in 2003

(paper related to FUSE observations is in preparation). However, the exposure time of that FUSE observation is relatively short. In order to demonstrate how our new method helps the joint analysis in the two bands, we use HST Cosmic Origins Spectrograph (COS) observations in 2009 instead, which has a good spectral resolution and a higher signal-to-noise ratio. The most likely origin of the WAs in Mrk 290 is from a slow torus wind (several 100 km s^{-1}), based on constraints from the X-ray band. Thus it is possible that the UV and X-ray observations reveal the same components even when the observations are separated by years.

The prevalent method in UV studies is to compare individual lines in velocity space. Information on different aspects of each absorption line, such as column density, ionization state, covering fraction, broadening, and saturation, is collected and combined to infer physical quantities of the outflowing gas. The process requires laborious work. In this work, we demonstrate a novel and simple method to combine the information from the UV and X-ray bands. We fit the UV spectra directly using synthetic spectral models generated by the XSTAR[1] photoionization code, the same modeling technique as was used for the X-ray data.

[1] http://heasarc.gsfc.nasa.gov/lheasoft/xstar/xstar.html

第二章　电离气体与模型

§2.1　电荷交换光谱软件ACX

Smith et al. (2012) have presented an approximate model for the CX process and the subsequent electrons cascading down in energy levels, resulting in a predicted emission spectral model. While the details can be found in the work by Smith et al. (2014) (or online[1]), we here present a brief outline of the model.

The model assumes the most probable CX process that only a single electron is captured by an ion. The process can be represented by

$$\mathrm{A}^{\mathrm{q}+} + \mathrm{N} \rightarrow (\mathrm{A}^{*})^{(\mathrm{q}-1)+} + \mathrm{N}^{+},$$

where a highly ionized ion $\mathrm{A}^{\mathrm{q}+}$ (such as O VIII and Ne X) picks up an electron from a neutral species N (H, H_2, or He), producing an excited ion $(\mathrm{A}^{*})^{(\mathrm{q}-1)+}$, which emits X-ray photons as it decays to the ground state.

The emission spectrum depends on the relative n and l distribution of the captured electrons, which affects the transitions during the subsequent electron cascade to the ground state. The principal n shell for the electron capture is determined from Equation (2.6) of Janev & Winter (1985). The orbital angular momentum l is more complex: several distributions are available, each roughly corresponding to different center-of-mass velocities of the system. At lower collision energies, the separable l distribution is suitable (Equation (3.59) of Janev & Winter 1985). Once captured, the electron cascades down to the ground state, purely by spontaneous or two-photon emission. The model calculation includes a complete set of ions and radiative transitions based on the AtomDB database (Foster et al. 2012). Therefore, the calculated emission spectrum can then be directly compared to an observed one.

We consider two extreme electron-capture modes regarding to whether an ion can have at most one CX. In one case, we assume that only one electron is captured. This is for CX in a sea of ions meeting occasional individual neutral atoms that have penetrated into the hot ``wind'', a circumstance suitable for the solar wind (Smith et al. 2014). In another

[1] www.atomdb.org/CX/

case, the ``standard'' one, multiple CX captures occur rapidly until the ion becomes neutral, an assumption justified by the large cross section for CX --typically several orders of magnitude higher than the electron--ion collisional excitation cross sections. The difference between the two cases is mainly reflected by the H- and He-like ion ratios (due to one or two CX captures) for C, N, O, and Ne. The prominent lines from Li-like ions usually have energies lower than 0.3 keV and therefore are not in an RGS spectrum.

The cold gas in the outflow of M82 is either clouds entrained by the hot gas or the inflows due to the interaction with M81 (Melioli et al. 2013). In the infrared band image of M82, the thickness of the filaments and shells of the cold gas are normally on the scale of several 10 pc (Engelbracht et al. 2006), much greater than the mean free path of the CX that occurs at the immediate vicinity of the interface due to its large cross section (typically a few $\times 10^{-15}$ cm^2). Thus, the situation in M82 is probably more suitable for the multiple CX case, in which the normalization parameter is physically meaningful as

$$\eta = 10^{-5} f_{\mathrm{H}} / [4\pi D_{\mathrm{A}}^2 (1+z)^2],$$

where D_{A} and z are the angular diameter distance and the cosmic redshift of the target, and $f_{\mathrm{H}} = \int n_{\mathrm{H}} v dS$ is the equivalent (metal abundance-dependent) hot proton incident rate (in units of $\mathrm{protons\,s^{-1}}$) through the interface. When the normalization is determined in a fit to the observed spectrum, f_{H} can then be measured. Furthermore, if the proton density n_{H} of the hot plasma and the velocity v (of ions relative to neutral atoms) can be estimated, one can then infer the effective area of the interface in the spectral extraction region.

§2.2 ACX的诊断分析

The CX spectrum is a entirely new spectrum, thus understanding some of its effects and characteristics would be beneficial. This section will discuss its radiative efficiency at different temperatures, as well as its special two-peak structure that can be displayed in soft X-ray CCD spectra.

2.2.1 辐射效率

We set up a simple scenario to help understanding the radiative efficiency of the CX process and its discrepancy from the thermal radiation. Consider that a cylinder, with a length of L and a bottom area of S, is filled with thermal plasma with a density of n and solar abundances, and the plasma moves at a velocity of v toward the top of cylinder where is a thick layer of cold gas. Then the luminosity of the thermal emission can be estimated

as

$$L_{(APEC)} = \Lambda_{(APEC)}\, 3.526 \times 10^{54}\, (\frac{n}{0.1})^2 (\frac{L}{10\,\mathrm{pc}})(\frac{S}{1\,\mathrm{pc}^2}),$$

and of the CX emission as

$$L_{(CX)} = Er_{(CX)}\, 4.761 \times 10^{43}\, (\frac{n}{0.1})^2 (\frac{v}{500\,\mathrm{km/s}})(\frac{S}{1\,\mathrm{pc}^2}),$$

where the $\Lambda_{(APEC)}$ is the cooling rate of thermal process and $Er_{(CX)}$ is the radiative efficiency of CX process. Taking values from the equations as L=10 pc, $S = 1\,\mathrm{pc}^2$, n=0.1, and v=500 km s^{-1}, we show in Figure 2.1 how the luminosities of the thermal and the CX emission on the soft X-ray band of 6-30 Å change with the temperature of the plasma. The luminosity of the thermal emission peaks around 1 keV and decreases quickly above 2 keV, while for the CX emission the luminosity increases monotonously with the temperature and becomes stable above 2 keV. The reason causing the large difference between the two processes is that, at the temperatures higher than 2 keV, most ions are fully stripped thus the collisional transition radiation is ineffective.

Both $Er_{(CX)}$ and $\Lambda_{(APEC)}$ depend only on the temperature, indicating the radiative capabilities of the two processes. Their ratio obtained as $Er_{(CX)}/\Lambda_{(APEC)} = (L_{(CX)}1.2nL)/(L_{(APEC)}v)$ ascends steadily and quickly above the temperature of 1 keV, as shown by the dash line in Figure 2.1. It suggests that, though the very hot plasma ($\geq$5 keV) has a weak and featureless thermal spectrum in the soft X-ray band, it still can be detected by the CX emission if colliding with cold gas.

2.2.2 独特的双峰结构

Normally, Fe XVII (17.1 Å) and Fe XVII (15.0 Å) are the strong lines in a thermal spectrum (Table 4.2). Combined with O VIII Lyβ, they contribute one strong peak around 0.8 keV in a APEC spectrum with CCD resolution, as shown in the left panel of Figure 2.2 that convolves a Chandra ACIS Redistribution Matrix (rmf file). However, the CX spectrum shows a distinctive two-peak structure under the same cylinder scenario in section 6.1. The left peak is O VII blent with O VIII Lyman α, while the right peak is the combination of Lyman β, γ, and δ. In CX process, the intensities of Lyman γ and δ lines are even stronger than Lyman β line, which is different from the thermal emission lines. And the two-peak structure is mainly due to the absent of strong iron L-shell lines, such as Fe XVII.

This phenomenon can be roughly explained by ion fractions. At the temperature of 0.6 keV, O^{+8}, the donor for CX O VIII lines, accounts for 94% of O ions, while the donor for CX Fe XVII lines Fe^{+17} occupies about 25% of all iron ions. In the thermal spectrum, O VIII lines are determined by O^{+7} that is about 6% of O ions, and Fe^{+16} for Fe XVII lines

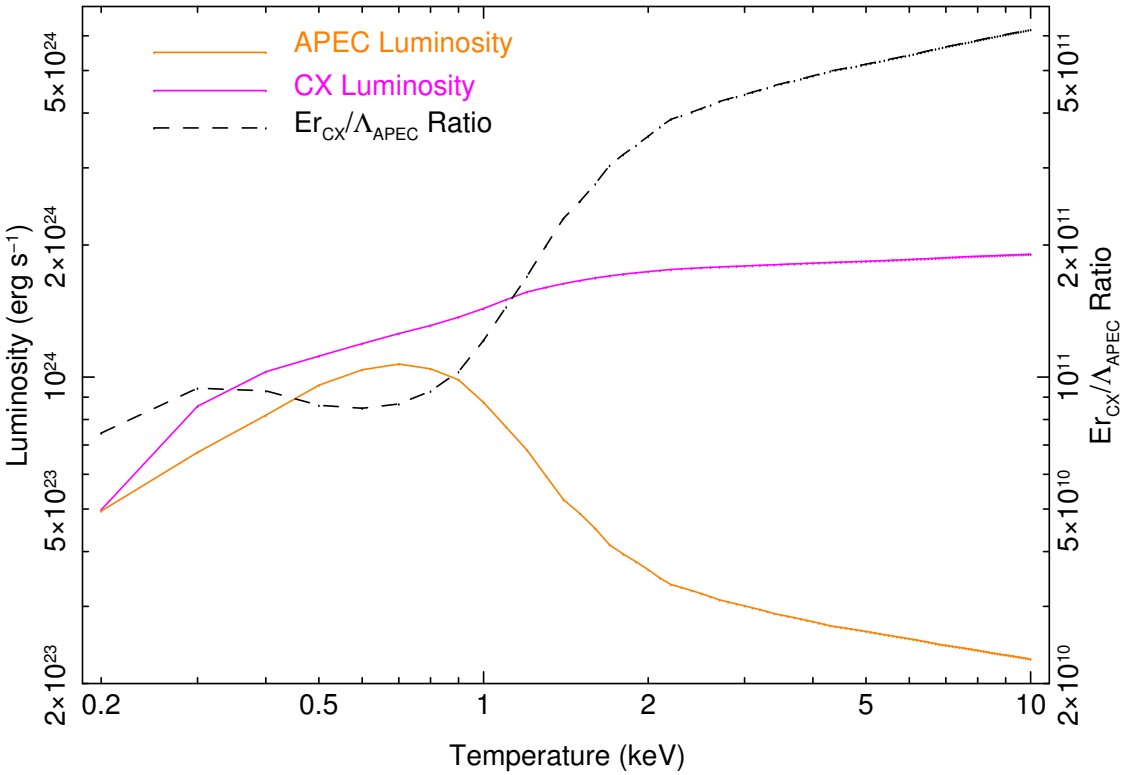

图 2.1 The orange and purple lines represent how the luminosities on 6-30 Å band contributed by the thermal and the CX emissions change with the plasma temperature, respectively. The detailed settings for estimating the luminosities are in the text. The dash line referring to the values on the right axis shows the ratio between the CX radiative efficiency and the thermal cooling rate that changes with the plasma temperature.

occupies 59% of iron ions. Regardless of any other issues, the O VIII lines appear about 40 times enhanced relative to the Fe XVII lines compared with the thermal case.

This special two-peak structure can be used in soft X-ray CCD spectral surveys to help quickly identify the existence of CX radiation. Therefore, it is important to check the stability of this structure, i.e. in which range of the temperature can it exist. A method to approach it is to check how the ratio of iron and O fluxes in 13-25 Å band changes with the plasma temperature. As seen in the right panel of Figure 2.2, the Fe/O flux ratio from CX radiation is always $\leq$0.15 for all temperatures. In contrast, the ratio from thermal radiation (APEC model) shows a prominent peak around 1 keV, and decreases quickly above 2 keV. However, since the branch ratio of O VIII Lyman α is much stronger than Lyman β, γ, and δ, the thermal spectrum would not show the two-peak structure in the 13-25 Å band even